Available online at www.sciencedirect.com

ScienceDirect

Proceedings of the Combustion Institute 000 (2018) 1–8

Proceedings of the Combustion Institute

www.elsevier.com/locate/proci

Large scale effects in weakly turbulent premixed flames

Pasquale Eduardo Lapenna [a,*], Rachele Lamioni [a], Guido Troiani [b], Francesco Creta [a]

[a] *Department of Mechanical and Aerospace Engineering, Sapienza University of Rome, Via Eudossiana 18, Rome, 00186, Italy*

[b] *ENEA C.R. Casaccia, via Anguillarese 301, 00123, Rome, Italy*

Received 29 November 2017; accepted 19 June 2018
Available online xxx

Abstract

In this study we numerically investigate large scale premixed flames in weakly turbulent flow fields. A large scale flame is classified as such based on a reference hydrodynamic lengthscale being larger than a neutral (cutoff) lengthscale for which the hydrodynamic or Darrieus–Landau (DL) instability is balanced by stabilizing diffusive effects. As a result, DL instability can develop for large scale flames and is inhibited otherwise. Direct numerical simulations of both large scale and small scale three-dimensional, weakly turbulent flames are performed at constant Karlovitz and turbulent Reynolds number, using two paradigmatic configurations, namely a statistically planar flame and a slot Bunsen flame. As expected from linear stability analysis, DL instability induces its characteristic cusp-like corrugation only on large scale flames. We therefore observe significant morphological and topological differences as well as DL-enhanced turbulent flame speeds in large scale flames. Furthermore, we investigate issues related to reaction rate modeling in the context of flame surface density closure. Thicker flame brushes are observed for large scale flames resulting in smaller flame surface densities and overall larger wrinkling factors.

Keywords: Large scale flames; Darrieus–Landau instability; Laminar premixed combustion; Turbulent premixed combustion; Direct numerical simulation

1. Introduction

Turbulent premixed combustion is a multiscale phenomenon involving disparate spatial and temporal scales. Indeed the premixed turbulent combustion regime diagram [1–3] distills the essential aspects of the flame-turbulence interaction by comparing relevant chemical and turbulent scales. This is however performed independently of the experimental or numerical configuration and, in particular, irrespective of whether the flame is constrained by a particular experimental device size or a numerical domain size L, which inherently represents the largest hydrodynamic length scale of the flow field to which the flame is subject.

This being said, the question arises as to whether the thermochemical properties of the mixture itself,

* Corresponding author.
E-mail address: pasquale.lapenna@uniroma1.it (P.E. Lapenna).

https://doi.org/10.1016/j.proci.2018.06.154
1540-7489

as well as the operating pressure, can introduce and modulate, in addition to the flame thickness, a further, larger length scale to be compared to L. This is indeed the case when considering the linear stability of a planar premixed flame. Darrieus [4] and Landau [5] original stability analysis ignored diffusive effects and found a deflagrative front to be unconditionally unstable, identifying the so-called hydrodynamic or Darrieus–Landau (DL) instability. Successive studies [6–8] incorporated thermal, molecular and viscous diffusion within the flame thickness and found, for Lewis numbers larger than a critical value, a potentially stabilizing quadratic term in the dispersion relation characterizing the growth rate ω of a disturbance of wavenumber k. For disturbances of sufficiently short wavelength, the DL mechanism is balanced by the stabilizing mechanism of diffusive nature. The cutoff (or neutral) wavelength λ_c, for which this occurs, thus introduces a mixture-dependent lengthscale which is generally far larger than the flame thickness. As a consequence, a flame constrained by a domain size $L > \lambda_c$ will be subject to large-scale effects due to the DL instability which a flame constrained by smaller domains will not experience.

Recent investigations have revealed a substantial difference in the morphological and propagative properties of large-scale ($L > \lambda_c$) compared to small scale flames. The characteristic flame wrinkling due to DL instability in large-scale flames was observed in both laminar and turbulent settings in multiple experimental [9–12] and numerical [13–18] studies. The DL induced morphology was found to be associated to an increase in flame area and to a consequent increase in laminar as well as turbulent propagation speed. The latter is an effect which, as observations tend to suggest, is mitigated at high turbulence intensity. In this context we note that direct numerical simulations specifically devoted to the investigation of large scale effects and their domain of influence have been so far limited to 2D configurations, with 3D studies conducted only in a weakly non linear scenario [19,20]. Moreover in a recent review, Sabelnikov and Lipatnikov [21] conjectured that for an unbounded statistically planar turbulent premixed flame, there exist a hierarchy of ever-growing cutoff wavelengths with respect to which the flame can be thought to be hydrodynamically unstable, irrespective of the thickness of the turbulent flame brush. This further motivates the investigation of large scale effects on turbulent premixed flames.

Drawing from the observations of previous studies, this work focuses on relevant features of large scale flames characterized by $L > \lambda_c$, and in particular how they compare to flames constrained by a hydrodynamic scale $L < \lambda_c$. To this end we first analyze the difference between large scale and high Karlovitz number simulations and secondly we investigate, by means of three dimensional direct numerical simulations (DNS), both large scale and small scale flames using two representative configurations, namely a statically planar flame and a slot bunsen flame. In such simulations the mixture dependent quantities are kept constant in order to have the same λ_c and thus to isolate the effects of L.

2. DNS of large scale flames

2.1. Large scale vs high Karlovitz simulations

Before addressing the features of large scale flames, it is useful to place them in the context of typical turbulent premixed flames and the relevant length scales that characterize them. To this end we begin by estimating a characteristic hydrodynamic cutoff length scale. The most complete dispersion relation, based on a general two reactant mixture, was derived in [22] and reads:

$$\omega(k) = \omega_0 S_L^0 k - \mathcal{D}_{th}\omega_1 k^2 = \omega_0 S_L^0 \frac{2\pi}{\lambda}\left(1 - \frac{\lambda_c}{\lambda}\right) \tag{1}$$

where ω_0 is a function of σ, the unburned to burned mixture density ratio and $\omega_1 = B_1 + Ze(Le-1)B_2 + PrB_3$, where Ze, Le and Pr are the Zeldòvich, Lewis and Prandtl numbers and $B_{1,2,3}$ are functions of σ (expressions can be found in [22]). The dispersion relation introduces a cutoff wavelength $\lambda_c = 2\pi\ell_D\omega_1/\omega_0$ where $\ell_D = \mathcal{D}_{th}/S_L^0$ is the diffusive length scale taken as a measure of flame thickness, with $\mathcal{D}_{th}$ the thermal diffusivity of the mixture and S_L^0 the unstretched laminar flame speed. The cutoff wavelength λ_c represents a length-scale dependent on the thermochemical properties of the mixture as well as pressure such that an unconstrained flame is hydrodynamically unstable to small perturbations of wavelength $\lambda > \lambda_c$. If the flame is constrained by the hydrodynamic length L, then the flame is unstable to perturbations of wavelength $\lambda_c < \lambda < L$. The latter instability condition translates to $\delta < \delta_c$ where $\delta = \ell_D/L$ is the flame thickness in units of L and $\delta_c = \ell_D/\lambda_c$ is a critical nondimensional flame thickness. In a recent study [17], the cutoff wavelength λ_c was estimated for propane-air mixtures using a number of available dispersion relations [7,22–24]. All models showed a moderate dependence of δ_c from equivalence ratio ϕ and resulted in an average estimate $\lambda_c \approx 160\ell_D$. Other estimates [14,25] using simpler models with constant transport properties across the flame, yielded lower estimates of $\lambda_c \approx 76\ell_D$ for propane-air mixtures ($\phi = 0.8$) and $\lambda_c \approx 56\ell_D$ for hydrogen-air mixtures ($\phi = 1.0$). In the context of recent experiments of freely propagating flames in tubes [9,26], the cutoff wavelength for propane-air mixtures, inclusive of gravity effects, was estimated as $\lambda_c \approx 0.8 \sim 0.4$ cm for $\phi = 0.8 \sim 1.4$, corresponding to $\lambda_c/\ell_D \approx 120 \sim 45$. In conclusion, a

Please cite this article as: P.E. Lapenna et al., Large scale effects in weakly turbulent premixed flames, Proceedings of the Combustion Institute (2018), https://doi.org/10.1016/j.proci.2018.06.154

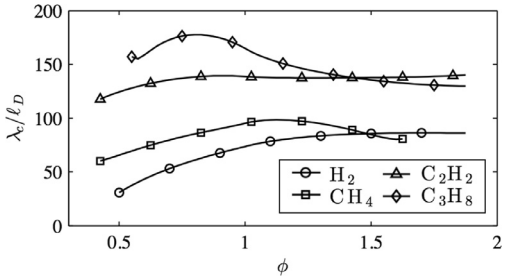

Fig. 1. Characteristic cutoff wavelength λ_c estimated numerically using Eq. (1) as a function of equivalence ratio ϕ scaled in terms of ℓ_D for various fuels.

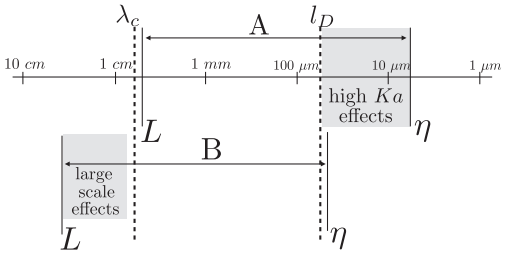

Fig. 2. Representative lengthscales involved in a (A) high-Ka and a (B) large scale turbulent premixed flame simulation. These representative simulations are characterized by the same mixture dependent quantities (λ_c and ℓ_D) and turbulent Reynolds number but different dimensions of both the integral scales ℓ_0 (usually of the order of L) and the Kolmogorov η lengthscales.

reasonable estimate of the characteristic cutoff wavelength, possibly restricted to near stoichiometric hydrocarbon-air mixtures, is $\lambda_c \approx 10^2 \ell_D$ as shown in Fig. 1.

It is now of interest to discuss the implications of the scale estimation λ_c/ℓ_D for DNS studies of turbulent premixed flames. Large scale flames with L larger than λ_c, for which instability effects are active, given a fixed separation between integral $\ell_0 \sim L$ and Kolmogorov η scales, can hardly be, concurrently, a flame characterized by an elevated Karlovitz number (high-Ka). Figure 2 exemplifies this scenario by displaying the range of lengthscales for two DNS of comparable scale separation and thus turbulent Reynolds number Re_0, exhibiting, respectively, high-Ka effects (for which $L > \lambda_c$) and large-scale effects due to hydrodynamic instability (for which $\ell_D > \eta$). Such effects, therefore, appear mutually exclusive, so that high-Ka simulations are relegated to small scale domains (typically smaller than λ_c) and generally high turbulence intensities whereas large scale simulations (larger than λ_c) are usually devoted to low Ka flames at low turbulence intensities. The concurrent presence of both effects, on the other hand, can be achieved only at the cost

Table 1
Mixture related parameters which are common for all the simulations presented.

σ	Le	Ze	Pr	δ_c	δ_T
3.0	1.2	6.0	0.1	0.0258	0.05

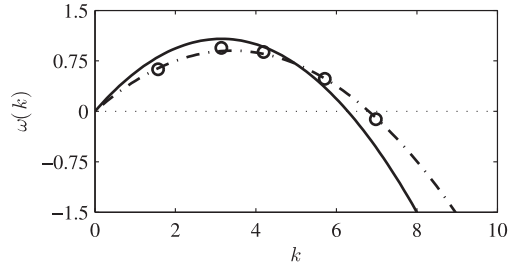

Fig. 3. Comparison between analytical (solid line) and numerical (circles simulations, dash-dotted line parabolic fit) dispersion relation. The values of $\omega(k)$ and k are made non-dimensional consistently with the dimensionless governing equations.

of keeping L fixed and dramatically increasing Re_0, hence reducing η for a given ℓ_0.

As an example, taking a representative subset of recent high-Ka DNS as a reference [27–29], it is of interest to note that the ratio between L and ℓ_D for such flames remains quite confined, being respectively $L/\ell_D \sim 28$ in [27], $L/\ell_D \sim 18$ in [28] and $L/\ell_D \sim 37$ in [29]. Based on the previous estimates for λ_c/ℓ_D, it is evident that in these simulations large scale effects are inherently inhibited.

2.2. Formulation and DNS setup

The formulation employed in this work has been extensively described in [17] and adopts a one-step irreversible Arrhenius reaction model in which the reaction rate is determined by a deficient reactant Y. The reaction progress variable is therefore defined as $c = 1 - Y$. The only difference between the formulation used in the present work and [17] consists in the nondimensionalization, now with respect to the cut-off wavelength λ_c, instead of the reference hydrodynamic length L, this resulting in δ_c replacing δ in the governing equations reported in [17]. The value of δ_c can be estimated for a particular mixture using Eq. (1). The mixture parameters used in the present work, defined in a standard manner are reported in Table 1. The Prandtl number is chosen as $Pr = 0.1$ in order to limit the dissipation rate of turbulent fluctuations from the inlet to the flame front. The evaluation of δ_c by means of Eq. (1) is numerically assessed by extracting the growth rate ω of a small disturbance as a function of the wave number $k = 2\pi/L$ in a 2D planar premixed flame configuration using various domains sizes. The comparison reported in Fig. 3 highlights

Please cite this article as: P.E. Lapenna et al., Large scale effects in weakly turbulent premixed flames, Proceedings of the Combustion Institute (2018), https://doi.org/10.1016/j.proci.2018.06.154

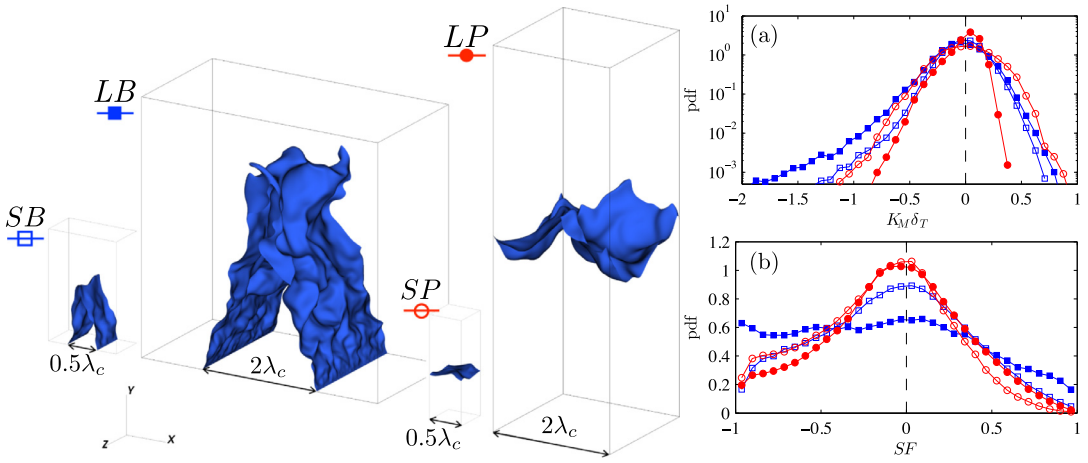

Fig. 4. Overview of flame morphology and computational domains, from left to right: small/large scale slot bunsen flame (SB/LB) and small/large scale statistically planar flame (SP/LP). Panel (a) pdf of the mean curvature K_M, panel (b) pdf of the shape factor SF, both variable are conditioned to c^*.

a good agreement between asymptotic theory and the numerical results.

Four low-Ka direct numerical simulations are performed, namely a small/large scale slot Bunsen flame (SB/LB) and a small/large scale statistically planar flame (SP/LP). The investigation is limited to weak turbulence, for which we expect DL-effects to be clearly visible and not overwhelmed by turbulent wrinkling. The small scale flames are characterized by domains with reference hydrodynamic length of $L = 0.5\lambda_c$ while for large scale flames $L = 2.0\lambda_c$ such that they are expected to be hydrodynamically unstable. The slot flame configuration consists in a square slot burner of width L surrounded by a hot coflow with a vertical velocity chosen in order to avoid shear between the two streams as described in [17]. A square slot burner has been chosen so that a single reference hydrodynamic length arises. The computational domain employed is a box of dimensions $L_x \times L_y \times L_z$ being $L_x = 2L$ and $L_z = L$ for both the slot flames while $L_y = 2L$ for LB and $L_y = 3L$ for SB. Dirichlet boundary conditions are imposed at the inflow, a slot bulk velocity $U_{bulk}/S_L^0 = 4.4$ is chosen with the superimposition of homogeneous isotropic turbulence (HIT) possessing prescribed $u_{rms}/S_L^0 = 1.1$ and $\ell_0/\lambda_c = 0.1$. Free-slip boundary conditions are used on the lateral side of the domain while outflow conditions are imposed at the upper boundary. The statistically planar flame is attained by means of an inflow/outflow configuration, in which flame stabilization is obtained by imposing an inflow velocity equal to the instantaneous turbulent burning velocity S_T [30]. A rectangular box of dimensions $L_x \times L_y \times L_z$ is used, being $L_x = L_z = L$ in the x and z homogeneous directions and $L_y = 3L$ in the propagation direction y. Superimposed to the bulk inflow velocity S_T, perturbations characterized by $u_{rms}/S_L^0 = 2.2$ and $\ell_0/\lambda_c = 0.1$ are added. The imposed HIT perturbations are identical between the large scale and the corresponding small scale flames. This fact, albeit artificial, allows us to perform a consistent comparison and to properly isolate large scale effects. Such perturbations have been obtained following [31] as illustrated in [32]. The computational domains and instantaneous realizations of a representative isosurface c^* are displayed in Fig. 4 while configuration and turbulence parameters are reported in Table 2.

Table 2
Configuration, inlet turbulence and relevant non-dimensional parameters of the 4 cases presented, namely small/large scale slot bunsen flame (SB/LB) and small/large scale statistically planar flame (SP/LP).

	SB	LB	SP	LP
L/λ_c	0.5	2.0	0.5	2.0
u_{rms}/S_L^0	1.1	1.1	2.2	2.2
ℓ_0/λ_c	0.1	0.1	0.1	0.1
η/λ_c	0.006	0.006	0.003	0.003
$Re_0 = u_{rms}\ell_0/\nu$	42.6	42.6	85.3	85.3
$Ka_L = \ell_D^2/\eta^2$	0.18	0.18	0.71	0.71
Plots legend	□	■	○	●

The simulations are carried out using a low-Mach number version [17,33] of the massively parallel flow solver `nek5000` [34] based on the spectral element method (SEM) [35]. The numerical discretization is uniform and the resolution kept constant for all of the four cases. Such resolution was chosen as $\Delta_E = \delta_T$ being Δ_E the lateral dimension of each spectral element and δ_T the thermal thickness of a 1D unstrecthed freely propagating flame, defined as $\delta_T = (T_b - T_u)/\max(dT/dx)$. The polynomial order N chosen for the

Please cite this article as: P.E. Lapenna et al., Large scale effects in weakly turbulent premixed flames, Proceedings of the Combustion Institute (2018), https://doi.org/10.1016/j.proci.2018.06.154

approximation of the solution within each element is $N = 8$, this resulting in approximately 9 grid points within δ_T. For all the cases investigated, statistics are collected during a complete flow-trough time starting sufficiently away from the initial laminar conditions. Averages in both time and homogeneous directions (x and z for the planar flame and only z for the slot) are denoted by an overbar $\overline{\cdot}$ while averages in time only are expressed as $\langle\cdot\rangle$. In the present work, conditional statistics are taken at $c^* = 0.64$, which corresponds to the progress variable value, on the fresh side, at which the reaction rate Ω is half of its maximum in the reference laminar, one-dimensional, unstretched planar flame. This value can be considered sufficiently close to the peak reaction zone to be used for a well posed flame characterization [36].

2.3. Flame morphology and topology statistics

A preliminary inspection of the flames in Fig. 4 reveals that highly curved crests and wide troughs, which delineate the characteristic DL-induced cusp-like morphology, are present only for LB and LP large scale cases. As expected, the weakly turbulent motions induce the large scale flames to lose stability while in the small scale cases stabilizing diffusive effects prevail. In the LP case the DL-induced cusp-like structures are visible over the entire flame surface while in the LB case, owing to the stabilization of the flame imposed by the slot configuration, the DL-induced corrugation is seen to develop and grow along the flame sides. In the small scale SB configuration, on the other hand, not enough convective time is available for any hydrodynamic instability to develop. In two dimensional simulations [17] cusp-like formations were detected in terms of localized bursts of negative flame curvature (flame normal oriented toward burnt gases) which they induce, as opposed to moderately positive curvature values along the troughs. The skewness of the flame curvature was thus identified as an unambiguous marker of the DL-instability presence. In the present three dimensional scenario similar considerations are expected to hold in terms of the mean curvature, defined as $K_M = (\kappa_1 + \kappa_2)/2$ being $\kappa_{1,2}$ the principal curvatures of an isosurface [37].

The mean curvature probability density function (pdf) conditioned to c^* is reported in panel (a) of Fig. 4 for all configurations. Consistently with classical literature results [38], the most probable K_M value is around zero for all cases. In particular the pdf's for the slot flames are easily interpretable, since the LB case shows a negative K_M tail that produces a more negatively skewed pdf profile than the SB case, which can be assumed to statistically indicate the presence of DL-induced cusp-like structures. Conversely, planar flames require more care in their interpretation. Indeed, the inflow/outflow configuration is characterized by a significant decay of inflow turbulence in the direction of flame propagation in weakly turbulent conditions [30]. Despite large and small scale configurations being supplied with identical HIT inflow perturbations, the SP case experiences a higher turbulence intensity due to shorter domain in the y direction resulting in smaller dissipation and thus a wider and symmetric pdf. On the other hand, while the LP case experiences a smaller turbulence intensity, resulting in a narrower curvature pdf, such pdf remains largely skewed towards negative curvatures due to the presence of DL-induced structures. This confirms that in a three dimensional setting, the skewness of the K_M pdf distribution (skew$(K_M) = -1.11, -1.09, -0.07, -0.46$ respectively for LP, LB, SP and SB) can still be used as a marker for detecting large scale effects which are manifested as DL-induced corrugation.

A useful characterization of the flame topology can be given by the pdf of the shape factor SF displayed in panel (b) of Fig. 4 where, given the two principal curvatures, SF is defined as the ratio between the principal curvature of smaller magnitude and the remaining curvature [37]. In the planar configuration the DL-induced morphology causes a decrease in the probability of a flame topology characterized by a negative SF toward the saddle regions ($SF = -1$) and, concurrently an increased probability of positive SF values toward spherical regions ($SF = 1$). The most probable topology (cylindrical shape $SF \sim 0$) remains essentially unaltered. Conversely, in the slot configuration, DL instability causes a substantial decrease in the probability of a flame topology being characterized by a cylindrical shape. Indeed the LB case shows an almost flat distribution over a wide range of SF values which slightly decrease when approaching spherical morphologies.

2.4. Burning velocities and flame surface densities

The DL-induced morphology described above is associated with a flame area increase which impacts on the laminar as well as turbulent propagation speed. Similar topological features can influence the flame area, such as unburnt mixture fingers [39] which, similarly to DL instability, are a manifestation of the interaction between the premixed flame and pressure field. However, contrary to DL instability, they are not related to λ_c and L, thus they are expected to be present in both large and small scale flames and to play a substantial role at higher turbulence intensity [21].

The impact of the morphological differences between large and small scale flames in a weakly turbulent environment are now quantified in terms of turbulent flame speeds. In LB and SB cases the turbulent burning velocity, as commonly done for envelop flames [40], has been calculated using the global consumption speed concept $S_{T,GC} = \dot{m}/\rho_u A_{\tilde{c}=c^*}$, being $\dot{m}$ the inlet mass flow rate and

Please cite this article as: P.E. Lapenna et al., Large scale effects in weakly turbulent premixed flames, Proceedings of the Combustion Institute (2018), https://doi.org/10.1016/j.proci.2018.06.154

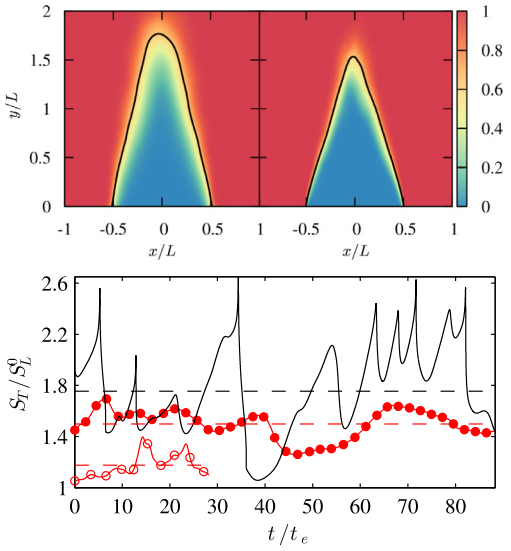

Fig. 5. Top panel: $\bar{c}$ fields for SB (left) and LB (right) cases, solid black lines indicate the c^* isoline used for $S_{T,GC}$ evaluation. Bottom panel: time evolution of turbulent flame speed S_T/S_L^0: LP (●), SP (○), and a 2D version of LP (–), the corresponding dashed lines represent $\langle S_{T,GC}\rangle$. The time t is normalized with the HIT eddy turnover time $t_e = \ell_0/u_{rms}$.

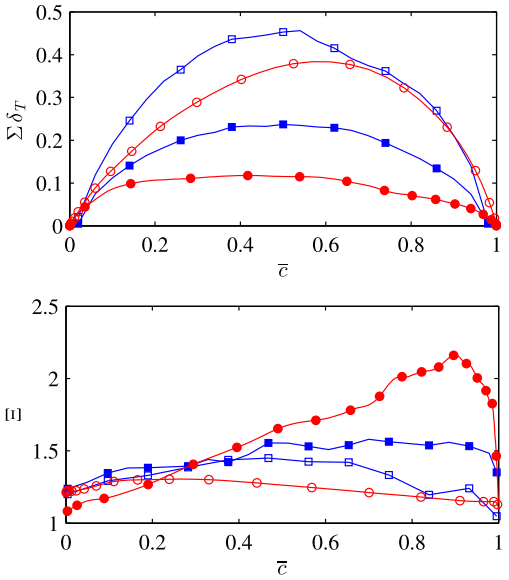

Fig. 6. Conditional averages of FSD (upper panel) scaled with the thermal thickness and wrinkling factor (lower panel): LB (■), SB (□), LP (●) and SP (○).

$A_{\bar{c}=c^*}$, the area of the averaged iso-contour $\bar{c} = c^*$. In LP and SP cases, the turbulent burning velocity is obtained via the volume integral of reaction rate of the progress variable $\dot{\omega}_c$ as $S_T = (\rho_u A_p)^{-1} \int_V \dot{\omega}_c dV$ being A_p the projected area in the direction of mean flame propagation [30].

The upper panel of Fig. 5 shows the averaged progress variable fields of the slot flames, rescaled with the reference hydrodynamic length, together with the c^* isoline used for the evaluation of $S_{T,GC}$. The LB case highlights a smaller rescaled mean flame height which leads to a higher global consumption speed $S_{T,GC}/S_L^0 = 1.36$ compared to the SB case $S_{T,GC}/S_L^0 = 1.17$, with a $\sim$16% increase usually denoted as a DL-enhancement. Although not shown, the enhancement calculated using 2D version of the LB and SB cases, is $\sim$19.5%. The lower panel of Fig. 5 shows the time evolution of S_T and the averaged value $\langle S_T\rangle$ scaled by S_L^0 for the LP and SP cases and, in addition, a 2D version of LP. The LP flame propagates faster ($\langle S_T\rangle = 1.50$) than SP ($\langle S_T\rangle = 1.18$) due to large scale effects although, as mentioned above, the turbulence intensity experienced by the two flames is different as is also evident from the time series of S_T/S_L^0. The latter finding is rather remarkable since it highlights that u'/S_L is not the only parameter upon which S_T/S_L^0 depends since, even if impacted by a lower turbulence intensity, large scale flames propagate faster. Moreover, the flame area increase and the ensuing DL-enhancement is far less evident than in 2D configurations being $\langle S_T\rangle = 1.75$ in the 2D LP case. The behavior of S_T for the two dimensional case is in accordance with other 2D DNS results [16]. The comparison between 2D and 3D can be further complicated by the different characteristics of the turbulence impacting the flame front. However, based on the results presented, we can partially conclude that, in a three dimensional scenario, DL-enhancement as a large scale effect is a less pronounced phenomenon.

Flame surface density (FSD) based reaction rate closure methods are well established in the context of both large eddy simulation (LES) and Reynolds averaged Navier-Stokes (RANS) approaches [38]. It is therefore of interest to understand how large scale effects can impact on its pivotal quantities, namely the generalized flame surface density, defined as $\Sigma = |\overline{\nabla c}|$, and the wrinkling factor, defined as $\Xi = |\overline{\nabla c}|/|\nabla \bar{c}|$ [41].

In order to consistently compare the investigated flames, because the two configurations used have a different number of inhomogeneous directions, we use conditional averages of Σ to the corresponding mean progress variable field $\bar{c}$, as shown in the upper panel of Fig. 6. It is clearly observable that large scale flames (LP and LB) compared to small scale flames (SP and SB) are characterized by lower values of Σ conditional averages. In particular, the DL-induced morphology produces a thicker flame brush which causes the flame surface to be spread over a wider spatial domain, thereby reducing its density. It is noteworthy that this trend is present in both the planar and slot

Please cite this article as: P.E. Lapenna et al., Large scale effects in weakly turbulent premixed flames, Proceedings of the Combustion Institute (2018), https://doi.org/10.1016/j.proci.2018.06.154

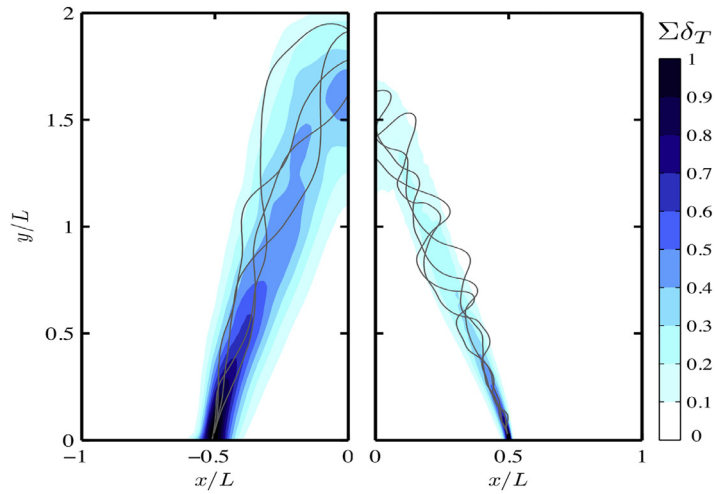

Fig. 7. Spatial distribution of Σ for SB (left panel) and LB (right panel) with superimposed four slices ($z = 0.5L$) of instantaneous realizations of the flame front identified by $c = c^*$. For clarity only half of the domain is shown in the x direction.

configurations investigated in the present work. The DL-enhancement resulting from the flame area increase, can be statistically viewed, similarly to Σ, by means of the conditional averages of Ξ which are reported in the lower panel of Fig. 6. Large scale flames, under similar weakly turbulent conditions compared to their small scale counterpart, are characterized by overall larger wrinkling factors. The described behavior is also evident in Fig. 7 displaying the spatial distribution of Σ for the slot flames. The higher degree of wrinkling of the large scale flame is clearly shown by the instantaneous 2D flame slices. This trend confirms the one described above for turbulent burning velocities since Ξ can be simply interpretable as $\Xi \sim S_T/S_L$. Indeed the larger Ξ values are presented by the LP case, i.e. the case with the higher turbulent to laminar burning velocity ratio. In the context of FSD based closure, Ξ is often modeled using algebraic relations based on local grid resolution, turbulence spectral properties and mixture parameters such as δ_T and S_L^0 (see for instance [41]). Drawing from the DNS results presented in this work the need of an additional mixture dependent parameter, expected to be related to λ_c, is evident in order to take into account large scale effects. Dedicated a-priori analysis on a wide range of chemical and turbulence parameters can be therefore envisaged to investigate large scale effects on turbulent combustion modeling.

3. Conclusion

We introduce the concept of large scale premixed flames for which the reference hydrodynamic length scale L is larger than the Darrieus–Landau cutoff scale λ_c. Large and small scale flames for constant Re_0 and Ka are investigated by means of 3D DNS in the context of two paradigmatic configurations, highlighting morphological, topological and propagative differences. Large scale effects on flame surface density based reaction rate modeling are also investigated.

The Darrieus–Landau induced cusp-like corrugation is observed only for large scale flames and the skewness of the mean curvature pdf is assessed as its morphological marker. An enhancement of the turbulent burning velocity is also observed, albeit less pronounced than in a two-dimensional setting, which can be attributed to the additional DL-induced wrinkling. Large scale flames exhibit thicker flame brushes, inducing smaller flame surface densities and overall larger wrinkling factors. This suggests that large scale effects should be incorporated in reaction rate flame surface density closure models in terms of mixture related corrections.

Future work will be dedicated to sub-unity Lewis number flames, which are expected to exhibit smaller cutoff lengthscales and, concurrently, additional small scale wrinkling due to thermal diffusive instabilities.

Acknowledgments

The authors acknowledge CINECA for computing resources (DL-DNS grant) and E. Lo Schiavo for part of post-process routines developed under the co-supervision of A. Attili and F. Bisetti.

Please cite this article as: P.E. Lapenna et al., Large scale effects in weakly turbulent premixed flames, Proceedings of the Combustion Institute (2018), https://doi.org/10.1016/j.proci.2018.06.154

References

[1] N. Peters, *J. Fluid Mech.* 384 (1999) 107–132.
[2] N. Peters, *Turbulent combustion*, Cambridge univ. press, 2000.
[3] A.N. Lipatnikov, J. Chomiak, *Progr. in Energ. Combust. Sci.* 36 (1) (2010) 1–102.
[4] G. Darrieus, *Unpublished work*. 1938.
[5] L.D. Landau, *Acta Phys. Chim. USSR* 19 (1944) 77–85.
[6] M.L. Frankel, G.I. Sivashinsky, *Combust. Sci. Technol.* 29 (3–6) (1982) 207–224.
[7] P. Pelce, P. Clavin, *J. Fluid Mech.* 124 (1982) 219–237.
[8] M. Matalon, B.J. Matkowsky, *J. Fluid Mech.* 124 (1982) 239–259.
[9] C. Almarcha, B. Denet, J. Quinard, *Combust. Flame* 162 (4) (2015) 1225–1233.
[10] C. Almarcha, J. Quinard, B. Denet, E. Al-Sarraf, J.M. Laugier, E. Villermaux, *Phys. Fluids* 27 (9) (2015) 091110.
[11] G. Troiani, F. Creta, M. Matalon, *Proc. Combust. Inst.* 35 (2) (2015) 1451–1459.
[12] S. Yang, A. Saha, F. Wu, C.K. Law, *Combust. Flame* 171 (2016) 112–118.
[13] C. Altantzis, C.E. Frouzakis, A.G. Tomboulides, M. Matalon, K. Boulouchos, *J. Fluid Mech.* 700 (2012) 329–361.
[14] N. Fogla, F. Creta, M. Matalon, *Combust. Flame* 162 (7) (2015) 2758–2777.
[15] C.E. Frouzakis, N. Fogla, A.G. Tomboulides, C. Altantzis, M. Matalon, *Proc. Combust. Inst.* 35 (1) (2015) 1087–1095.
[16] R. Yu, X.-S. Bai, V. Bychkov, *Phys. Rev. E* 92 (6) (2015) 063028.
[17] F. Creta, R. Lamioni, P.E. Lapenna, G. Troiani, *Phys. Rev. E* 94 (5) (2016) 053102.
[18] R. Lamioni, P.E. Lapenna, G. Troiani, F. Creta, *Flow Turb. Combust.* https://doi.org/10.1007/s10494-018-9936-0 (2018).
[19] B. Denet, *Phys. Fluids* 16 (4) (2004) 1149–1155.
[20] F. Creta, N. Fogla, M. Matalon, *Combust. Theo. Model.* 15 (2) (2011) 267–298.
[21] V.A. Sabelnikov, A.N. Lipatnikov, *Ann. Rev. Fluid Mech.* 49 (2017) 91–117.
[22] M. Matalon, C. Cui, J.K. Bechtold, *J. Fluid Mech.* 487 (2003) 179–210.
[23] P. Clavin, P. Garcia, *Journal de Mécanique Théorique et Appliquée* 2 (2) (1983) 245–263.
[24] F. Creta, M. Matalon, *Proc. Combust. Inst.* 33 (1) (2011) 1087–1094.
[25] N. Fogla, F. Creta, M. Matalon, *Combust. Flame* 175 (2017) 155–169.
[26] J. Quinard, G. Searby, B. Denet, J. Graña Otero, *Flow Turb. Combust.* (2012) 1–17.
[27] S. Lapointe, G. Blanquart, *Combustion and Flame* 167 (2016) 294–307.
[28] H. Wang, E.R. Hawkes, B. Zhou, J.H. Chen, Z. Li, M. Aldén, *Proceedings of the Combustion Institute* 36 (2) (2017) 2045–2053.
[29] T. Nilsson, H. Carlsson, R. Yu, X.-S. Bai, *Fuel* 216 (2018) 627–638.
[30] M. Klein, N. Chakraborty, S. Ketterl, *Flow Turb. Combust.* (2017) 1–17.
[31] L. Davidson, M. Billson, *Int. J. Heat Fluid Flow* 27 (6) (2006) 1028–1042.
[32] P.E. Lapenna, F. Creta, *J. Sup. Fluids* 128 (2017) 263–278.
[33] P.E. Lapenna, R. Lamioni, P.P. Ciottoli, F. Creta, Low-Mach number simulations of transcritical flows, *2018 AIAA Aerospace Sciences Meeting, AIAA SciTech Forum, (AIAA 2018-0346)*, 2018.
[34] PF Fischer, JW Lottes, SG Kerkemeier, http://nek5000.mcs.anl.gov (2008).
[35] A.T. Patera, *J. Comput. Phys.* 54 (3) (1984) 468–488.
[36] G.K. Giannakopoulos, A. Gatzoulis, C.E. Frouzakis, M. Matalon, A.G. Tomboulides, *Combust. Flame* 162 (4) (2015) 1249–1264.
[37] S.B. Pope, P.K. Yeung, S.S. Girimaji, *Phys. Fluids A* 1 (12) (1989) 2010–2018.
[38] T. Poinsot, D. Veynante, *Theoretical and numerical combustion*, RT Edwards, Inc., 2005.
[39] A.N. Lipatnikov, J. Chomiak, V.A. Sabelnikov, S. Nishiki, T. Hasegawa, *Proc. Combust. Inst.* 35 (2) (2015) 1401–1408.
[40] J.F. Driscoll, *Prog. Energ. Combust. Sci.* 34 (1) (2008) 91–134.
[41] N. Chakraborty, M. Klein, *Phys. Fluids* 20 (8) (2008) 085108.

Please cite this article as: P.E. Lapenna et al., Large scale effects in weakly turbulent premixed flames, Proceedings of the Combustion Institute (2018), https://doi.org/10.1016/j.proci.2018.06.154